NUMERICAL STUDY OF COMPRESSION AND HEATING OF CONICAL TARGETS

V. V. Demchenko and A. S. Kholodov

UDC 518:517.9:533.9

1. In recent years, among other problems of laser thermonuclear synthesis (LTS) there has been great interest in so-called "conical" targets [1-7], in which the thermonuclear fuel is compressed and heated in a conical cavity in heavy material (lead, etc.) with the aid of a shell section accelerated by a laser pulse (Fig. 1). It can be expected that the basic features of the flow pattern will be similar to the case of compression and heating of shell microtargets. The main advantages of using such targets are the following: The action of the laser radiation is applied not to an entire sphere, but only a relatively small solid angle, which simplifies creation of a more homogeneous laser spot; the laser energy attainable is concentrated on a significantly smaller surface, permitting increased energy flux and simulation of the situation which will exist when more powerful lasers are developed; the implosion duration is increased, because the same mass as in the case of a spherical shell can be located at much greater distances from the center ($\sim$1000 μm), so that the work is performed over a much longer path, which markedly reduces the peak power requirements of the laser pulse. There is no doubt that such targets also have drawbacks. When the aperture angle of the conical cavity is too small, target heating and compression can be affected significantly by the products of evaporation of the cavity walls, even to the point of their coating the channel and cutting off the shell segment from the laser beam. Questions arise as to the effect of conditions in the wall region on stability of target material compression, on the behavior of the heavy material in the final stage of the process, in particular, on formation and size of the cavern at the peak of the conical target, etc.

The present study will present some results of two-dimensional calculations (using Euler variables) of such targets, performed on the basis of the conservative variant of the grid-characteristic method of [9] proposed in [8]. As in [8], the mathematical model of the physical processes occurring in the high temperature plasma includes absorption of external laser radiation (in the one-dimensional formulation along radial directions), the hydrodynamic motion, electron thermal conductivity, and electron–ion collision relaxation. The basic system of two-dimensional non-steady-state equations of the two-temperature plasma was presented in [8], and was supplemented by an equation for the mass concentration ξ of one of the components of the two-component mixture of ideal gases

$$\frac{\partial(\rho\xi)}{\partial t}+\frac{1}{\Delta}\left[\frac{\partial(S_{23}\rho u\xi)}{\partial\theta}+\frac{\partial(S_{13}\rho v\xi)}{\partial r}\right]=0.$$

This equation was solved for the hydrodynamic motion stage using the method of splitting the calculation among physical processes described in [8]. Here $\Delta = H_1H_2H_3$; $S_{13} = H_1H_3$, $S_{23} = H_2H_3$ are geometric parameters characterizing the elementary volume and its surface: H_1, H_2, H_3, Lamé coefficients; ρ, density; u, v, azimuthal and radial components of the velocity vector; θ, r, spherical coordinates. The thermophysical properties of the plasma (specific heats at constant volume, c_e, c_i, absorption coefficient K, thermal conductivity coefficient κ_e, etc.) are determined by the usual method for a multicomponent mixture, i.e., as functions of the density ρ, electron and ion temperature T_e, T_i, and mass concentration ξ. As has already been noted, the external laser energy flux is taken homogeneous over azimuthal angle θ and acts only within the limits of the conical cavity. The integral region (in the Euler variables θ, r) includes some portion of the conical cavity together with the shell (of thickness s) $R_0 - \delta_1 \le r \le R_0 + \delta_2$ and a portion of the volume occupied by the heavy material (lead with a density of 13.5 g/cm^3 for the calculations), $0 \le \theta \le \theta_* + \delta_3$ and was varied (by choice of $\delta_1(t)$, $\delta_2(t)$, $\delta_3(t)$) as the process developed so that it encompassed practically the entire mass of material set into motion (both shell and lead, see Fig. 1). As in

Moscow. Translated from Zhurnal Prikladnoi Mekhaniki i Tekhnicheskoi Fiziki, No. 6, pp. 131-138, November-December, 1985. Original article submitted June 15, 1984.

0021-8944/85/2606-0877$09.50

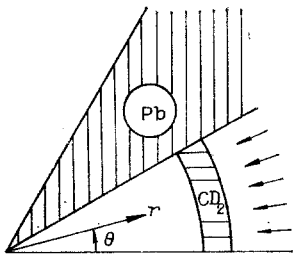

Fig. 1

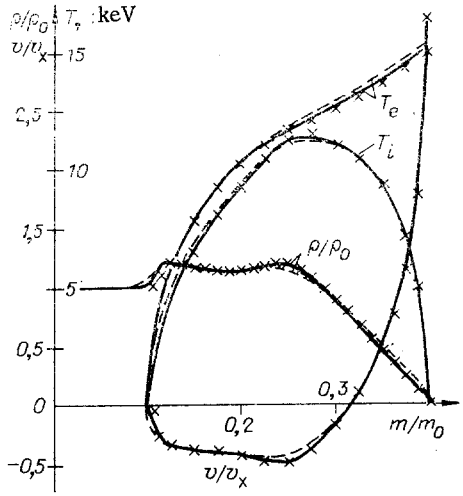

Fig. 2

[8], the exterior boundary of the integration region $R_0 + \delta_2(t)$ was chosen to reduce a to a minimum the effect of low density mass which leaves the integration region.

2. Before analyzing the results obtained for conical targets, we will briefly compare data obtained for one-dimensional problems obtained using the conservative variant of the grid-characteristic method [8] using both Euler variables and Lagrangian mass coordinates with the calculations of Samarskii et al., performed in Lagrange variables using a completely conservative implicit method [10, 11].

For LTS problems in which motion of a finite mass of material is considered, methods using Lagrange variables are most widespread, in particular for one-dimensional problems, where the advantages of that approach related to automatic grouping of the difference grid nodes in regions with high density are obvious. Euler variables are preferable for significant shear deformations of the material, possible in multidimensional problems, since in a number of cases they permit a more detailed description of absorption of the external laser radiation in the low density "crown" of the disintegrating portion of the target material, where in the traditional Lagrangian approach it is quite difficult to insure the necessary spatial step in the difference grid (as well as near the center of the target). In addition, in a number of cases with Euler variables it is difficult to insure the necessary detail in the difference grid in the region with high material density, especially in problems involving very thin shells.

In the one-dimensional case, when the Lagrangian mass coordinate m is chosen such that $dm = \rho r^\nu dr$ the system of equations used for the calculations takes on the form

$$\frac{dr}{dt} = v; \tag{2.1}$$

$$\frac{\partial (1/\rho)}{\partial t} - \frac{\partial (r^\nu v)}{\partial m} = 0; \tag{2.2}$$

$$\frac{\partial v}{\partial t} + r^\nu \frac{\partial p}{\partial m} = 0; \tag{2.3}$$

$$\frac{\partial E}{\partial t} + \frac{\partial (r^\nu v p)}{\partial m} + \frac{\partial (r^\nu q)}{\partial m} = \frac{\partial}{\partial m}\left(r^{2\nu} \varkappa_e \rho \frac{\partial T_e}{\partial m}\right) - Q_{ei}/\rho; \tag{2.4}$$

$$\frac{\partial \varepsilon_i}{\partial t} + p_i \frac{\partial (r^\nu v)}{\partial m} = Q_{ei}/\rho, \tag{2.5}$$

where in analogy to [8] the laser radiation flux density $q(t, m) = q_r(t) \exp(-\int_m^{m_g} (K/\rho r^\nu)\, dm$; $Q_{ei} = Q_0 \rho^2 (T_e - T_i)/T_e^{3/2}$ is the exchange term; $E = \varepsilon_e + \varepsilon_i + v^2/2$ is the total energy; $p = p_e + p_i$ is the pressure ($p_{e,i} = (\gamma - 1)\rho$); $\varepsilon_{e,i}$ is the internal energy of electron and ion components ($\varepsilon_{e,i} = c_{e,i} T_{e,i}$); γ is the adiabatic index; $\nu = 0$, 1, 2, for planar, cylindrical, and spherical geometries. The left (hyperbolic) portion of system (2.1)-(2.5) can be approximated by an

explicit difference scheme of first order accuracy [8], a scheme with positive approximation which gives a monotonic solution for calculations of flows with discontinuities within the integration region and is stable given fulfillment of the Courant–Friedrichs–Levy condition $\tau \leq h/\max |\lambda_i|$, where λ_i are eigenvalues of the matrix A of the original system (2.1)-(2.5)

$$\partial w/\partial t + A(t, m, w)\partial w/\partial m = f(t, m, w).$$

The right side of system (2.1)-(2.5), which makes the original system parabolic and includes terms with electron thermal conductivity and exchange term Q_{ei}, is approximated by an implicit scheme in order to avoid the limit on integration step $\tau \sim h^2$ characteristic of finite schemes for parabolic equations.

When Euler variables (t, r) are used the form of the original system (2.1)-(2.5) and the choice of unknown parameters $w = \{\rho, \rho v, \rho E, \rho\varepsilon_i\}$ change somewhat, which changes the difference relationships in the scheme of [8], together with the integration region and corresponding boundary conditions.

Calculations for a number of one-dimensional problems involving compression of planar and spherical solid microtargets and spherical shells were performed using the formulation described above. Some of the results of these caclculations are presented in Fig. 2-6.

For a planar DT target (initial density $\rho_0 = 0.2$ g/cm^3) Fig. 2 compares calculations performed in Lagrangian mass coordinates with the conservative variant of the grid-characteristic method (CGC) (solid curves, integration step $h = \Delta m/m_0 = 0.004$; dashes $\Delta m/m_0 = 0.008$) to Kosarev's second order accuracy explicit completely conservative method [8], similar to the well known method of Samarskii [10, 11] (crosses in Fig. 2, $\Delta m/m_0 = 0.01$). At time $t = t_i = 1$ nsec (where t_i is the duration of the triangular laser pulse) profiles of density ρ/ρ_0, and electron T_e (keV) and ion T_i (keV) temperatures are shown together with dimensionless velocities v/v_X ($v_X = r_X/t_i = 10^9$ cm/sec). The laser pulse energy density $\mathscr{E} = 6.6 \cdot 10^7$ J/cm^2 and other defining parameters correspond to the calculations performed in [12].

The data on Figs. 3 and 4 were obtained for compression and heating of a 10% spherical shell of CD_2 ($\rho_0 = 1$ g/cm^3) by a trapezoidal laser pulse (Fig. 4) $t_i = 0.1$ nsec long with total energy E = 300 J. The initial shell radius $R_0 = 100$ μm. Parameter profiles are shown for the time t = 0.036 nsec (Fig. 3) together with time dependences of maximum values of density ρ_{max}, density of the inner shell boundary ρ_c and density at the center of the target ρ_c (Fig. 4). Shown are calculations with Lagrangian mass variables (total number of difference grid nodes M = 50) by the CGC method (solid lines) and by the implicit fully conservative method [10, 11], as performed at the Applied Mechanics Institute, Academy of Sciences of the USSR (dashes). As in the preceding variant, the agreement of the results is completely satisfactory.

Two-dimensional problems were modeled numerically using the method of [8] with Euler variables, so it is of interest to compare this method with data of other methods using the same type of variables. Some results of such a comparison with calculations performed at the Applied Mechanics Institute, Academy of Sciences of the USSR, by the method of [10, 11] are shown in Figs. 5 and 6 for a solid spherical target of CD_2 (Fig. 5, triangular pulse $t_i = 1$ nsec duration and total energy E = 300 J, initial sphere radius $R_0 = 55$ μm) and a 10% shell of CD_2 (same variant as Figs. 3 and 4). The solid curves of Figs. 5 and 6 are calculations by the CGC method in Euler variables, while the dashes are Applied Mechanics Institute data (Lagrange variables) with parameter profiles at time t = 0.5 nsec and $t = t_i = 0.1$ nsec, respectively. On the whole, the agreement of the data is completely satisfactory, although the method of [8] with Euler variables does not reproduce certain details in the density profile, in particular, the additional compression of the target material between the shock wave front and the thermal front, seen in the calculations with Lagrange variables (the density maximum second from the left in Fig. 5). The maximum density value in the target material is reproduced much more poorly for shell problems than in calculations with Lagrange variables (although the mean values in the compressed portion of the shell practically coincide, Fig. 6). In addition, the calculations in Euler variables produce a better expressed front in the shock wave traveling toward the center, which in the physical coordinates (t, r) is quite smeared in Lagrangian mass variables, because in regions with low density and also near the center of the target in spherical geometry the difference grid is less fine than in a continuous medium and away from the target center.

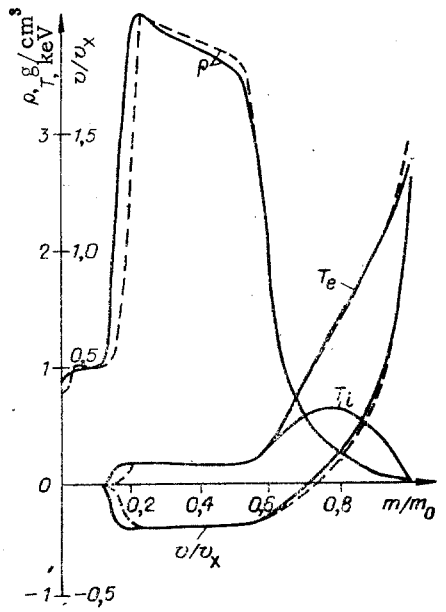

Fig. 3

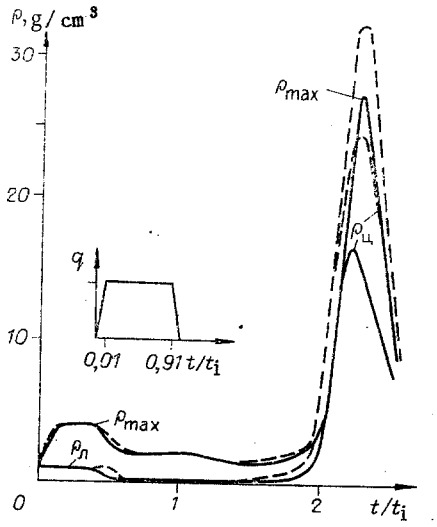

Fig. 4

The comparisons presented above show that the method of [8] produces results fully usable for the given class of problems, including those in Euler variables, and can serve as a base for study of various multidimensionl effects which develop upon compression and heating of microtargets by laser radiation.

3. One-dimensional calculations of compression and heating of microtargets (including "conical" ones) allow quite detailed reproduction of the major features of the phenomena being considered, evaluation of the effect of certain physical processes, optimization of targets, etc., however, questions related to the real multidimensional character of problems remain open. Some of these effects related to the multidimensional nature of the problem for conical targets are illustrated by Figs. 7-13.

Figures 7 and 8 show data corresponding to the initial stage of interaction of a laser pulse with a conical target with the following parameter values: semiaperture of conical cavity in lead $\theta_* = 7.5°$, thickness of CD_2 shell ($\rho_0 = 1$ g/cm^3) $\delta = 3$ μm, external shell radius $R_0 = 1000$ μm, duration of triangular pulse $t_i = 25$ nsec, total pulse energy E = 600 J. At time t = 0.25 nsec, when the shock wave formed by the laser pulse action exists to the outer boundary of the shell $r = R_0 - \delta$, we present the velocity field (Fig. 7), isobars p/p_X = const ($p_X = \rho_0 R_0^2/t_c^2$) and pressure distribution along the radial directions $\theta = 0$, $\theta = \theta_* = 7.5°$ and azimuthal direction r = 999 μm (Fig. 8, dash–dot line, initial position of conical cavity boundary). It is evident that near the boundary with the lead the compression wave (formed ahead of the thermal front) exists onto the internal boundary of the shell earlier. Outside the wall region the parameter distribution in the azimuthal direction is practically homogeneous and the interaction pattern is the usual one for shell problems: radial motion of the compressed portion of the spherical segment toward the center with expulsion of a hot low density plasma into a "crown." As is evident from the velocity field presented in Fig. 7, in the region near the wall there is a pattern in the azimuthal direction similar to that in the radial directions: propagation of the compression wave in the lead, evaporation and flow into the conical cavity of lead vapor. The interaction in the wall region of perpendicular "radial" and "azimuthal" jets of the evaporation products of the spherical segment and the lead form an elevated pressure zone in this region (Fig. 8), which leads to an earlier exit of the "radial" compression wave onto the internal boundary of the shell segment near $\theta = \theta_*$. In this stage of laser pulse action when plasma expulsion occurs into a practically undeformed "cylindrical" channel, the pressure in the "crown" along the radial directions θ = const changes slightly.

A similar pattern in the initial stage of laser pulse action on a spherical segment located in a conical lead cavity can be observed for other values of the problem parametes. The data presented in Figs. 9-13 correspond to the case $\theta_* = 25°$, $\delta = 2$ μm, $R_0 = 1726$ μm, rectangular pulse duration $t_i = 20$ nsec at a radiant flux density $q_g(t) \equiv q_0 = 6 \cdot 10^{13}$ W/cm^2.

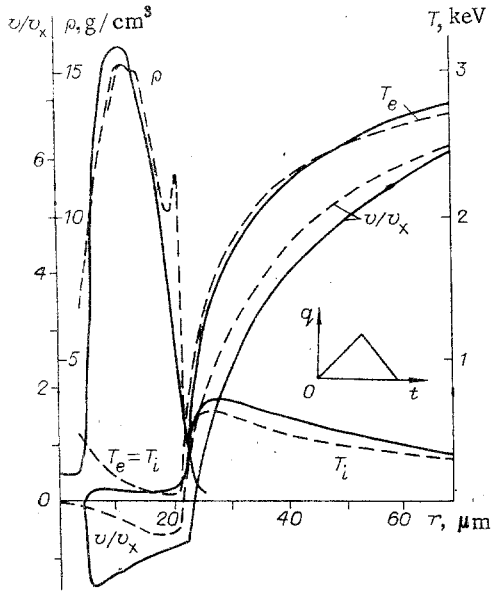

Fig. 5

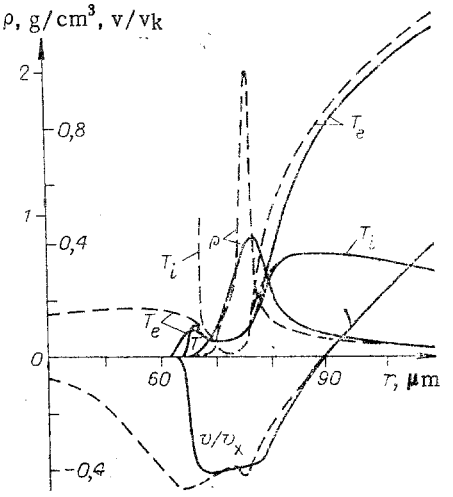

Fig. 6

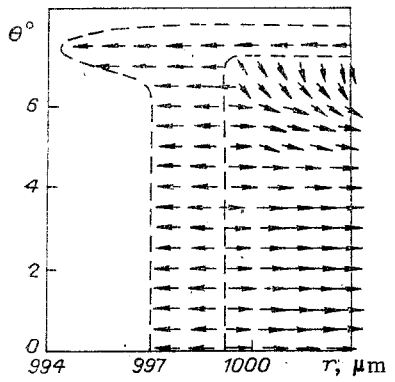

Fig. 7

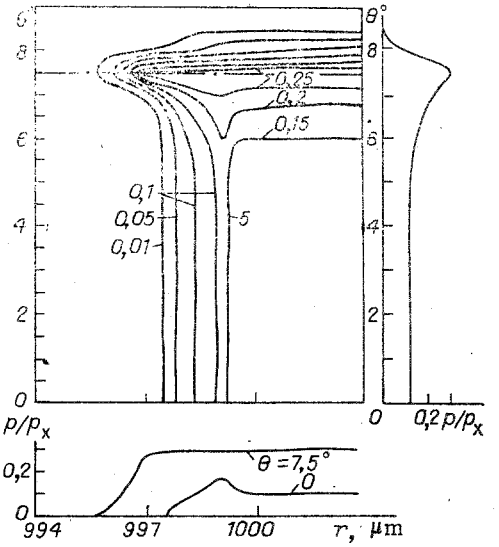

Fig. 8

The spherical film and residual gas filling the conical cavity are CD_2. For this variant Semenov's method with an implicit fully conservative scheme [10, 11] in Lagrangian variables was used to perform calculations in a one-dimensional formulation to evaluate the effect of multidimensionality and use of Euler variables in the two-dimensional calculations using the conservative variant of the grid-characteristic method [8].

At the stage when the spherical segment reaches the peak of the conical cavity the initial flow pattern described above is maintained. As is evident from comparison of the density and velocity profiles, as well as the electron T_e (keV) and ion T_i (keV) temperatures (Fig. 9) along the axis of asymmetry $\theta = 0$ at time $t = 10.3$ nsec (briefly before arrival of the shock wave at the peak of the conical cavity), on the whole the two-dimensional flow near the axis of symmetry (solid curves) agrees with the results of one-dimensional calculations (dashes), in particular, with regard to position of the shock and thermal wave fronts and the intervening shell position, etc. The greatest difference is in the peak value of shell density (when the values of mass moving toward the center are sufficiently close to each other), which is caused by the use of Euler variables in the two-dimensional numerical calculation, and has already been noted in the comparison of one-dimensional calculations for spherical shells discussed in Sec. 2.

For time $t = 10.5$ nsec Figs. 10 and 11 show isochors of $\rho(g/cm^3) = \text{const}$ and isotherms $T_e = \text{const}$, with the dashed lines being concentration isolines $\xi = 0.1$ (upper curves) and

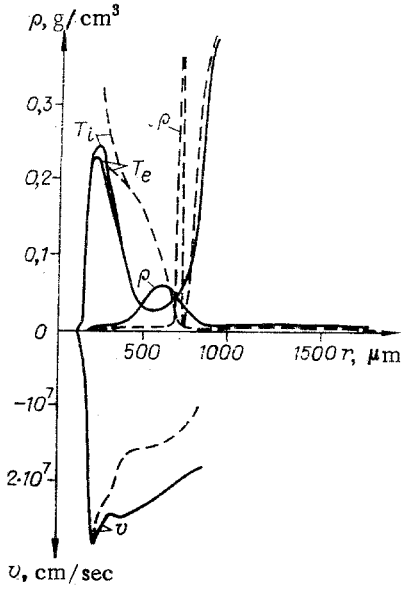

Fig. 9

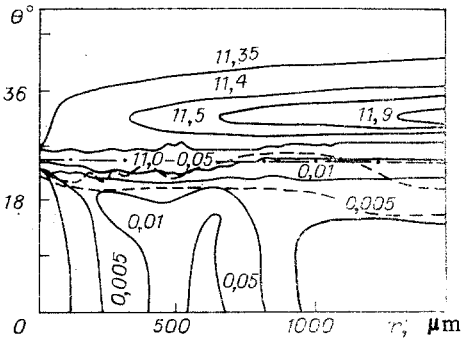

Fig. 10

$\xi = 0.9$ (lower), which convey the current position and form of the boundary with the lead, while the dash–dot lines are the initial boundary of the conical cavity.

In this stage of motion of the spherical segment toward the center the following basic features can be distinguished. Remaining relatively cold, the shell moves toward the center ahead of the thermal wave front, increasing markedly in thickness ("spreading"). A shock wave propagates ahead of the shell in the low intensity gas, always gaining over the shell. In a large portion of the conical cavity adjacent to the axis of symmetry the flow is radial and close to one-dimensional (the azimuthal components of the velocity field are much smaller than the radial). The two-dimensional nature of the flow appears basically near the boundary with the lead, where, as in the initial stage, the shock wave motion toward the center gains over the shell near this boundary (the velocity of the shock wave front near the boundary with the lead is markedly higher than near the flow's axis of symmetry). The difference in velocity of various sections of the shell itself is much less: near the axis it moves on the average even somewhat faster, as is indicated, for example, by the isoline $\rho = 0.05$ in Fig. 10. There are two relatively hot regions: the "crown," where the electron and ion temperatures are approximately the same and of the order of 0.5 keV, and the region directly behind the shock wave front, where because of the low density the ion and electron temperatures differ, especially so near the boundary with the lead. The portion of the shock wave moving in the radial direction near the boundary with the lead initially reaches the peak of the conical cavity, elevating the temperature and pressure there, so that as in the case of compression and heating of microtargets with harmonic perturbations of their form considered in [8], there is a tendency toward formation of turbulent motion in the central portion of the conical cavity between its peak and the shell moving toward the center. In the "crown" region the lead evaporation products partially fill the peripheral portion of the cavity (as can be seen by the displacement relative to the axis $\theta = 0$ of the isolines $\xi = \text{const}$), although on the whole this portion of the conical cavity is filled by products of evaporation of the shell segment, i.e., closing of the channel does not occur. A compression wave propagates within the lead.

In this stage of shell segment motion in the conical cavity the most interesting feature is the development of instability in the boundary with the lead in the region between the shock wave front and the thermal front, as indicated by the behavior of the line $\xi = 0.1$ here (Figs. 10 and 11). This phenomenon recalls Kelvin–Helmholtz instability and is practically absent in the "crown" region (behind the thermal front), where parameters are fully leveled by electron thermal conductivity. On the whole, the deformation of the conical cavity in this stage is relatively small, and in a first approximation such problems can be modeled by corresponding one-dimensional calculations up to the arrival of the shock wave at the cavity peak.

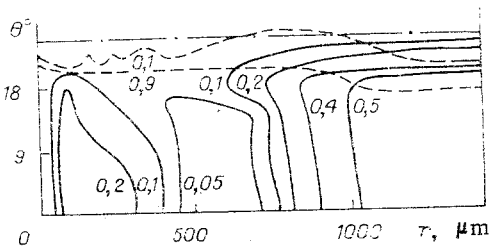

Fig. 11

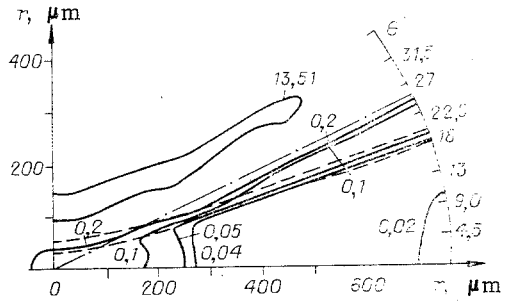

Fig. 12

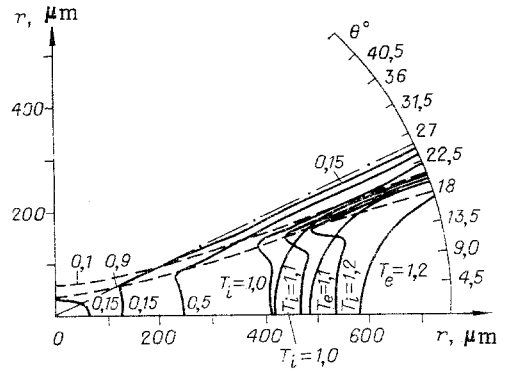

Fig. 13

The final stage of compression and heating of the spherical segment in a conical cavity is shown in Figs. 12 and 13, where for the time t = 14.9 nsec we present isochors ρ (g/cm^3) = const and isotherms T_e = const and T_i = const, the dashed lines are concentration isolines ξ = 0.1 and 0.9, and dash–dot lines are the initial position of the boundary with the lead. As is evident from the isolines ρ = const in this stage at the peak of the conical cavity a depression is formed in the lead – a cavern which at time t = 14.9 nsec has a size of $\sim$ 50 μm (Fig. 12), closed on the cavity side by fragments of the shell at a distance r $\sim$ 100-150 μm, beyond which there is a thermal wave front with low density "crown" at a temperature of $\sim$ 1 keV. The temperature of the plasma in the cavern is $\sim$ 0.3 keV, the density is of the order of tens of g/cm^3, i.e., the compression is relatively low, due to formation of a shock wave which outdistances the main mass of the shell segment and heats the gas in the conical cavity before arrival of the shell at the central part of the target. The peripheral portion of the conical cavity is deformed quite weakly, while the load evaporation products do not flow further into the cavity than the line θ = 18°, which is evident from the behavior of the isolines ξ = const, which have a form close to lines θ = const in this portion of the conical cavity.

Thus, in laser pulse compression and heating of thin segments located within a conical cavity in heavy material, the characteristic features observed by numerical modeling of the problem in a two-dimensional formulation are: formation of a region of increased pressure in the wall layer in the initial moments of laser pulse action and earlier exit of the compression wave formed ahead of the thermal wave front and propagating within the target onto

the internal boundary of the shell segment in the area near the wall; unstable behavior of the boundary with the lead (Kelvin–Helmholtz type instability) on the segment between the shock wave front advancing relative to the main segment mass and the thermal wave front at the stage where the shell segment is driven to the peak of the conical cavity; formation and development of a depression (cavern) in the heavy material near the peak of the conical cavity with slight overall deformation of the peripheral part of the conical cavity; flow into the peripheral part of the conical cavity of products of wall evaporation, but without complete filling of the channel.

LITERATURE CITED

1. G. S. Fraley and R. J. Mason, "Preheat effects on microballoon laser-fusion implosions," Phys. Rev. Lett., 35, No. 8 (1975).
2. R. J. Mason, D. V. Brockway, and E. L. Lindman, "2-d implosion of structured pellets for laser fusion," Los Alamos Report LA-VR-76-2319 (1976).
3. V. I. Vovchenko, A. S. Goncharov, et al., "Generation of thermonuclear neutrons by laser action on conical targets," Pis'ma Zh. Eksp. Teor. Fiz., 26, No. 9 (1977).
4. H. Derentowicz, S. Kaliski, et al., "Generation of thermonuclear fusion neutrons by means of a pure explosion. II. Experimental results," Bull. Acad. Pol. Sci. Ser. Sci. Tech., 25, No. 10 (1977).
5. S. I. Anisimov, V. I. Vovchenko, et al., "Study of the process of thermonuclear neutron generation by laser action on a conical target," Pis'ma Zh. Tekh. Fiz., 4, No. 7 (1978).
6. V. V. Demchenko and A. S. Kholodov, Gas and Conical Targets. Analytical Solutions [in Russian], NTO MFTI, Moscow (1979).
7. M. D. Taran, V. F. Tishkin, et al., "Modeling of collapse of quasispherical targets in solid state cones," Preprint, IPM Akad. Nauk SSSR, No. 127 [in Russian] (1980).
8. O. M. Belotserkovskii, V. V. Demchenko, et al., "Numerical modeling of some problems in laser compression of shells," Zh. Vychist. Mat. Mat. Fiz., 18, No. 2 (1978).
9. K. M. Magomedov and A. S. Kholodov, "Construction of difference systems for hyperbolic type equations on the basis of characteristic relationships," Zh. Vychisl. Mat. Mat. Fiz., 9, No. 2 (1969).
10. A. A. Samarskii, P. P. Volosevich, et al., "Finite difference method for solution of one-dimensional nonsteady state problems in magnetic hydrodynamics," Zh. Vychisl. Mat. Mat. Fiz., 8, No. 5 (1968).
11. A. A. Samarskii and Yu. P. Popov, Difference Methods in Gas Dynamics [in Russian], Nauka, Moscow (1975).
12. Yu. V. Afanas'ev, N. G. Basov, et al., "Heating of a deuterium–tritium plasma to thermonuclear temperatures with use of a laser," Preprint FIAN Akad. Nauk SSSR, No. 66 [in Russian] (1972).